Fundamental Frequency Response Bounds of Direct-Form Recursive Switched-Capacitor Filters with Capacitance Mismatch

Antonio Petraglia, *Senior Member, IEEE*

***Abstract*—A theoretical statistical analysis is developed to investigate the effects of random capacitance matching errors in the frequency response of recursive switched-capacitor filters implemented in direct form. As a result, with appropriate approximations, closed-form solutions for the mean and the standard deviation of the frequency response error are derived. The obtained expressions provide insight into the quantitative influence of capacitance ratio tolerance, numerator and denominator orders, passband and stopband ripples, and edge frequencies, and reveal existing tradeoffs among these parameters, so that the most efficient filter design can be found. The main theoretical results are extensively verified by simulation through Monte Carlo analysis to show the effectiveness of the proposed formulas.**

***Index Terms*—Capacitance mismatch, direct form, statistical sensitivity analysis, switched-capacitor filters, yield estimation.**

I. Introduction

THERE exists a variety of recursive (IIR) switched-capacitor (SC) filter structures, each having particular virtues and limitations. The direct-form realizations are deemed to have, in some situations, a distinctive edge over other implementations. The large number of high-quality SC delay lines presented in the literature, e.g., [1]–[4], makes it possible for a SC recursive filter to be efficiently implemented by two SC arrays—one in the forward path realizing the numerator coefficients and the other in the feedback path realizing the denominator coefficients—sharing one SC delay line, as illustrated in Fig. 1(a) [5]–[7]. The use of two (or more) SC delay lines, as shown in Fig. 1(b), has also been reported, e.g., to reduce total capacitance [8], to design structurally all-pass SC filters for low sensitivity realization of a transfer function [9], [10], and to implement SC decimation filters [11]. An approach employing a smaller number of operational amplifiers, multiplexed in time, has been recently described [12]. These direct-form structures offer a number of additional attractive features to the analog sampled-data designer, such as savings in power consumption and silicon area, facility for time-multiplexing common filter sections among several signals [13], and rejection of MOS amplifier noise and power-supply noise below the Nyquist frequency [6], [14].

Manuscript received April 2000; revised February 2001. This work was supported in part by CNPq/Brazil, Proc. 521090/98–9. This paper was recommended by Associate Editor G. Cauwenberghs.

The author is with the Electrical Engineering Department, University of California, Los Angeles, CA 90095 USA, on leave from the Federal University of Rio de Janiero, Rio de Janiero, Brazil.

Publisher Item Identifier S 1057-7130(01)04198-2.

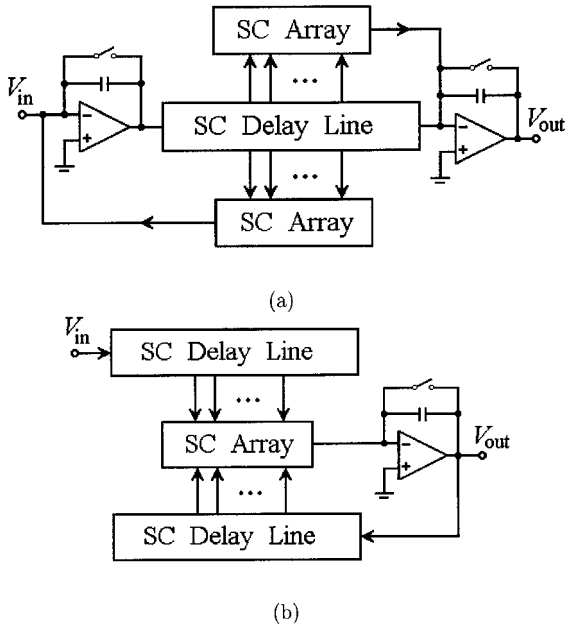

Fig. 1. Basic structures of recursive SC filters in direct form. (a) Using one delay line shared by two (forward and feedback) SC arrays. (b) Using two (forward and feedback) SC delay lines.

The disadvantage of direct realizations, opposed to other implementations, becomes clear in narrow-band filtering applications, where most of the poles are clustered near the unit circle. Then, the frequency response degradation due to the accumulation of pole deviations caused by coefficient errors can become quite large. Because of this pole-dependent coefficient sensitivity, direct realizations of recursive SC filters have their accuracy in the frequency response limited by capacitance ratio errors, as their coefficients depend on the matching characteristics of capacitor arrays. Other important nonideal factors include capacitive parasitics, switch charge injection, and finite operational amplifier gain and bandwidth, but their effects are less dependent of the filter structure. Moreover, these can be reduced by several techniques widely reported in the literature. As device dimensions continue to be scaled down, however, capacitance matching becomes increasingly difficult, leading to distortions in the frequency response. In a typical MOS process, edge uncertainties and oxide thickness variations introduce random errors affecting capacitance ratios that cannot be corrected by matching techniques [15]. These random errors, therefore, may be responsible for the ultimate limitation on the performance of direct-form recursive SC filters. One of the purposes of this

paper is to access the consequent degradation in the frequency response.

Deterministic analysis, based on the computation of derivatives of the filter transfer function with respect to capacitance ratios, can be used to estimate the mean and the standard deviation of the frequency response error [16], [17]. More accurate estimates may be obtained by computer-aided simulations using Monte Carlo methods, but these approaches only enable the designer to estimate the frequency response deviation of a given design, and consequently do not provide dynamic insight into the quantitative influence of parameters such as numerator and denominator orders, passband and stopband ripples, edge frequencies, and capacitance ratio tolerances.

In this paper, the effects of random capacitance ratio errors are formulated as a statistical problem, as in Monte Carlo methods, but are studied analytically, leading to closed-form expressions for the mean and the standard deviation estimates of the error in the frequency response. As shown by several illustrative examples, these estimates agree very closely with those provided by Monte Carlo simulations. As a result, the boundaries of the feasible frequency responses for a given nominal design and capacitance ratio tolerances are described mathematically, enabling yield estimation without any need for computer simulations. Besides establishing fundamental performance bounds, this paper indicates how the derived expressions can be used, along with an algorithm for the optimum design of recursive transfer functions [18], to find the most efficient filter solution in the sense that minimum (not necessarily equal) number of poles and zeros and maximum yield can be achieved. Also shown in this paper, when relatively large stopband attenuation is required, low sensitivity can be obtained in both passband and stopband by using a recursive SC structure implemented by lower order (typically second-order) nonrecursive [finite-impulse response (FIR)] SC sections [12].

This paper is outlined as follows. Mathematical models for random capacitance ratio errors are discussed in Section II. The estimates for the mean and the standard deviation of the error in the frequency response of nonrecursive SC filters are briefly reviewed in Section III. The statistical analysis of recursive SC filters is then developed in Section IV, where the resulting theoretical estimates are compared to their respective Monte Carlo estimates for a variety of transfer functions. Also verified in Section IV is the accuracy of the improved capacitance ratio error model proposed in Section II. An estimate for the achievable stopband attenuation is derived in Section V. Frequency response boundaries are derived in Section VI for yield evaluation and comparison. Concluding remarks are presented in Section VII.

II. Capacitance Ratio Error Modeling for Statistical Analysis

Various error mechanisms affecting MOS capacitances, for different working conditions, have been studied. Capacitance matching precision depends on the fabrication technology and is limited by systematic and random errors. The former can be significantly reduced by applying some proper layout techniques [19]. By using two arrays of unit capacitances interleaved in a common centroid geometry layout, for example, the resulting capacitance ratio accuracy is typically about 0.5%, and accuracies better than 0.1% have been experimentally obtained for actual integrated circuit implementations [19], [20]. The remaining uncertainty is mainly due to random variations of the manufacturing process and cannot be reduced by improved layout rules.

Random errors in capacitance ratios have been modeled as additive Gaussian random variables having zero mean and a standard deviation that depends on the nominal ratio value [20]–[22]. Accordingly, a mathematical model commonly used in computer-aided analysis of SC filters [16] to statistically describe random capacitance ratio errors is $\hat{\gamma}_k = \gamma_k + \epsilon_{\gamma_k}$, where $\epsilon_{\gamma_k} = \gamma_k \epsilon_k$, γ_k are capacitance ratios, and the ϵ_k are uncorrelated zero-mean Gaussian random variables. If the filter coefficients are realized by arrays of unit capacitances, then γ_k are rational numbers and ϵ_k are unit capacitance ratio errors.

Alternative models have been used with the purpose of obtaining a mathematically tractable problem that can be solved in closed form. In [23], the model $\epsilon_{\gamma_k} = \gamma_{\max} \epsilon_k$ has been considered in the analysis of random coefficient error effects in the frequency response of transversal filters realized by bucket brigade delay lines, where $\gamma_{\max}$ is the maximum coefficient value. The model $\epsilon_{\gamma_k} = \epsilon_k$, similar to the digital filter case except that ϵ_k are Gaussian random variables, has been used to investigate coefficient inaccuracy effects in SC transversal filters [24]. This model is also adequate for other analog signal-processing techniques [25], as, for example, the interesting design scheme proposed in [26], where each transfer function coefficient is given in terms of a pulsewidth only. In this case, coefficient inaccuracies are caused by rise- and fall-time errors and are, therefore, independent of the nominal pulse duration time.

In this paper, we adopt the model $\epsilon_{\gamma_k} = \overline{\gamma} \epsilon_k$ [27], where $\overline{\gamma}$ is the arithmetic mean of the absolute values of the filter coefficients, that is, $\overline{\gamma} = \sum_k |\gamma_k| / L$. This takes into account the fact that usually, as the filter length increases, the spread in the tap weight values and, consequently, in the capacitance ratios, becomes larger. Monte Carlo sensitivity analyses of SC filters having Gaussian random errors in their coefficients have shown (see Section IV) that $\overline{\gamma} \epsilon_k$ is a very good approximation to the more accurate model $\gamma_k \epsilon_k$.

A. Notation and Preliminary Assumptions

The mean and the standard deviation of a frequency-dependent random variable, say, $r(\omega)$, are here denoted as $\mu_r(\omega)$ and $\sigma_r(\omega)$, respectively. For simplicity of presentation, the analysis is developed for low-pass filters; it can be easily extended to other types of filter specifications. For the transfer function $H(\omega)$ of a low-pass filter with ideal components evaluated on the unit circle, it is assumed that $1 - \delta_p \leq |H(\omega)| \leq 1$ for all frequencies in the passband, given by $\Omega_p = [0, \omega_p]$, and that $|H(\omega)| \leq \delta_s$ for all frequencies in the stopband, given by $\Omega_s = [\omega_s, \pi]$, where $\delta_p = 1 - |H(\omega_p)|$ and $\delta_s = |H(\omega_s)|$.

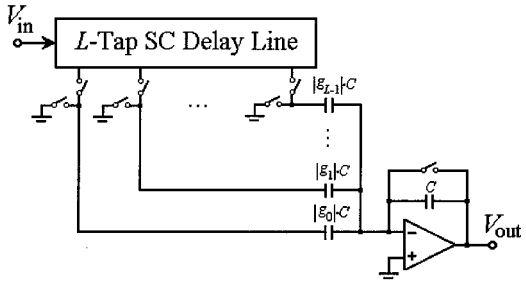

Fig. 2. Example of a SC realization of (1). Clock phases (not shown) depend on the signs of the corresponding coefficients g_k.

III. Nonrecursive SC Filters

The frequency response of a nonrecursive SC filter of length L can be written as

$$G(\omega) = \sum_{k=0}^{L-1} g_k e^{-j\omega k}. \tag{1}$$

It is assumed that each coefficient (or tap weight) $g_k, k = 0, 1, 2, \ldots, L-1$, is implemented as a ratio between two capacitances, as in the transversal structure of Fig. 2, or in other realizations using multiplexed op-amps [2]. In Fig. 2, the negative coefficients are realized by a proper choice of the corresponding switch clock phases (omitted for generality). Due to random capacitance errors introduced by the manufacturing process, the actual transfer function becomes

$$\begin{aligned}\hat{G}(\omega) &= \sum_{k=0}^{L-1} (g_k + \epsilon_{g_k}) e^{-j\omega k} \\ &= G(\omega) + \sum_{k=0}^{L-1} \epsilon_{g_k} e^{-j\omega k}\end{aligned} \tag{2}$$

where ϵ_{g_k} is the error associated with the nominal value of the kth capacitance ratio $|g_k|$. Thus, the deviation in the frequency response is

$$\begin{aligned}\Delta G(\omega) &= \hat{G}(\omega) - G(\omega) \\ &= \sum_{k=0}^{L-1} \epsilon_{g_k} e^{-j\omega k}.\end{aligned} \tag{3}$$

In [24], the analysis was carried out by substituting $\epsilon_{g_k} = \epsilon_k$ in (3), where ϵ_k, $k = 0, 1, 2, \ldots, L-1$, were assumed uncorrelated Gaussian random variable having zero mean and standard deviation σ_ϵ. As stated in the previous section, here we use $\epsilon_{g_k} = \overline{g}\epsilon_k$, where $\overline{g} = \sum_{k=0}^{L-1} |g_k|/L$ is the arithmetic mean of the capacitance ratios realizing the filter coefficients. Following the analysis in [24], it can be shown that $|\Delta G(\omega)|$ can be accurately modeled by a Rayleigh random variable with a mean value

$$\mu_{|\Delta G|}(\omega) = \frac{\sigma_g \sqrt{\pi L}}{2} \qquad \forall \omega \tag{4}$$

and a standard deviation

$$\sigma_{|\Delta G|}(\omega) = \frac{\sigma_g \sqrt{(4-\pi)L}}{2} \qquad \forall \omega \tag{5}$$

where $\sigma_g = \overline{g}\sigma_\epsilon$.

IV. Statistical Analysis of Recursive SC Filters

Equations (4) and (5) provide a quantitative way of evaluating the effects of random capacitance errors on the frequency response of SC nonrecursive filters and indicate that the mean and the standard deviation of $|\Delta G(\omega)|$ are approximately independent of the frequency. Distortions in the frequency response of recursive SC filters, on the other hand, are further aggravated by the fact that inaccuracies in pole locations are more critical than in zero locations. In particular, the pole closest to the unit circle exerts major influence in the region around the passband edge frequency, augmenting the deviation in the passband and reducing the attenuation in the stopband. How large the number of poles and zeros can be chosen before the frequency response reaches a prohibited level of distortion is one of the answers provided by the following analysis.

The transfer function of a recursive SC filter, evaluated on the unit circle, can be written as

$$H(\omega) = \frac{A(\omega)}{B(\omega)} \tag{6}$$

where

$$A(\omega) = \sum_{k=0}^{M-1} a_k e^{-j\omega k} \quad \text{and} \quad B(\omega) = 1 - \sum_{k=1}^{N-1} b_k e^{-j\omega k}. \tag{7}$$

Let ϵ_{a_k} and ϵ_{b_k} be random errors representing fluctuations around the nominal values of a_k and b_k, respectively. Then the poles and the zeros of the actual transfer function will differ from the desired poles and zeros, leading to a deviation $\Delta H(\omega)$ in the frequency response. The actual transfer function can thus be written as

$$\begin{aligned}\hat{H}(\omega) &= H(\omega) + \Delta H(\omega) \\ &= \frac{A(\omega) + \Delta A(\omega)}{B(\omega) + \Delta B(\omega)}\end{aligned} \tag{8}$$

where

$$\Delta A(\omega) = \sum_{k=0}^{M-1} \epsilon_{a_k} e^{-j\omega k} \quad \text{and} \quad \Delta B(\omega) = \sum_{k=1}^{N-1} \epsilon_{b_k} e^{-j\omega k}. \tag{9}$$

After multiplying both the numerator and denominator of (8) by $B(\omega) - \Delta B(\omega)$, and neglecting the terms $\Delta A(\omega)\Delta B(\omega)$ and $(\Delta B(\omega))^2$, the deviation $\Delta H(\omega)$ in the frequency response of the recursive filter can be approximated as

$$\Delta H(\omega) \approx \frac{\Delta A(\omega) - H(\omega)\Delta B(\omega)}{B(\omega)}. \tag{10}$$

Since $\Delta A(\omega)$ and $\Delta B(\omega)$ are deviations in the frequency responses of transversal filters with lengths M and $N-1$, respectively, then according to (4)

$$\mu_{|\Delta A|}(\omega) = \frac{\sigma_a \sqrt{\pi M}}{2} \quad \text{and} \quad \mu_{|\Delta B|}(\omega) = \frac{\sigma_b \sqrt{\pi (N-1)}}{2} \tag{11}$$

where $\sigma_a = \overline{a}\sigma_\epsilon$, $\sigma_b = \overline{b}\sigma_\epsilon$, and $\overline{a}$ and $\overline{b}$ are the arithmetic mean values of the capacitance ratios implementing the coefficients

of the respective transversal filters, that is, $\overline{a} = \sum_{k=0}^{M-1} |a_k|/M$ and $\overline{b} = \sum_{k=1}^{N-1} |b_k|/(N-1)$.

Before turning to the derivation of the mean and standard deviation of $|\Delta H(\omega)|$, we note that M and N assume values with the same order of magnitude, and in most cases $M = N$. Also, the transfer function coefficients are scaled in such a way that in the passband $|H(\omega)| \approx 1$ and the independent term of $B(\omega)$ is equal to one. Thus, for transfer functions with poles sufficiently close to the unit circle, we have $\overline{b} \gg \overline{a}$ (see examples in Sections IV-A and V-A), and consequently, it follows from (11) that $\mu_{|\Delta B|}(\omega) \gg \mu_{|\Delta A|}(\omega), \forall \omega \in \Omega_p$. As a result, the expected value of the magnitude of the deviation in the frequency response of $H(\omega)$ for frequencies in the passband is, from (10)

$$\mu_{|\Delta H|}(\omega) \approx \frac{\mu_{|\Delta B|}(\omega)}{|B(\omega)|} = \frac{\sigma_b \sqrt{\pi(N-1)}}{2|B(\omega)|} \qquad \forall \omega \in \Omega_p. \tag{12}$$

For frequencies in the stopband, $|H(\omega)| \leq \delta_s \ll 1$, so that

$$\mu_{|\Delta H|}(\omega) \approx \frac{\mu_{|\Delta A|}(\omega)}{|B(\omega)|} = \frac{\sigma_a \sqrt{\pi M}}{2|B(\omega)|} \qquad \forall \omega \in \Omega_s \tag{13}$$

where we have also assumed that $\overline{a}\sqrt{M} \gg \overline{b}\delta_s \sqrt{N-1}$ (see examples in Sections IV-A and V-A).

Similarly, using (5), we obtain for the standard deviation of $|\Delta H(\omega)|$ in the passband

$$\sigma_{|\Delta H|}(\omega) \approx \frac{\sigma_b \sqrt{(4-\pi)(N-1)}}{2|B(\omega)|} \qquad \forall \omega \in \Omega_p \tag{14}$$

and in the stopband

$$\sigma_{|\Delta H|}(\omega) \approx \frac{\sigma_a \sqrt{(4-\pi)M}}{2|B(\omega)|} \qquad \forall \omega \in \Omega_s. \tag{15}$$

The above formulas can be used to access the statistical variation in the particular frequency response of choice, by evaluating them at each frequency of interest. This is shown in Sections V and VI. They are next compared to their respective Monte Carlo estimates considering two capacitance ratio error models discussed in Section II and three different filter specifications to verify the effectiveness of the theoretical statistical analysis.

A. Monte Carlo Simulations

Monte Carlo estimates have been obtained by computing, at each given frequency ω_i, the sample mean

$$\eta\{|\Delta H(\omega_i)|\} = \frac{1}{K} \sum_{k=1}^{K} |\hat{H}_k(\omega_i) - H(\omega_i)| \tag{16}$$

and the sample standard deviation

$$\varsigma\{|\Delta H(\omega_i)|\} = \left[\frac{1}{K} \sum_{k=1}^{K} |\Delta H(\omega_i)|^2 - (\eta\{|\Delta H(\omega_i)|\})^2 \right]^{1/2} \tag{17}$$

of the error in the frequency responses of $K = 10\,000$ samples of SC filters $\hat{H}_k(\omega)$, $k = 1, 2, \ldots, K$, having Gaussian distributed capacitance ratio errors with zero mean and unit standard deviation $\sigma_\epsilon = 0.001$. The Monte Carlo estimates (16) and (17) for, respectively, the mean and the standard deviation of $|\Delta H(\omega_i)|$ have been compared to their corresponding theoretical estimates in (12)–(15). Some illustrative examples are presented next. In all plots, solid lines correspond to the theoretical expressions in (12)–(15). Results of Monte Carlo simulations are indicated by "$\circ$" for the capacitance ratio error model $\epsilon_{g_k} = \overline{g}\epsilon_k$ used in the theoretical analysis and by "$\star$" for the more realistic model $\epsilon_{g_k} = g_k\epsilon_k$. The latter is included with the purpose of verifying the accuracy of the model used in the theoretical analysis. The ideal frequency response, in dotted lines, corresponds to a transfer function without coefficient errors and is presented with the purpose of showing passband and stopband frequency regions.

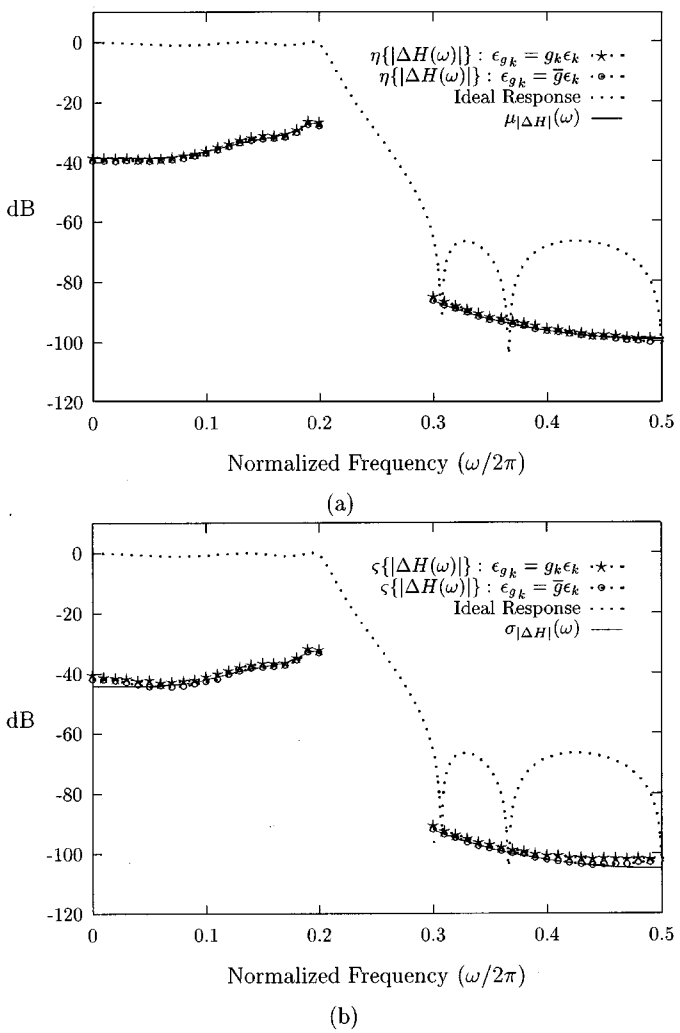

Fig. 3. Theoretical (solid lines) and Monte Carlo ("$\star$" and "$\circ$") estimates for (a) the mean and (b) standard deviation of $|\Delta H(\omega)|$ for the fifth-order elliptic filter of Example 1. Ideal frequency response shows passband and stopband.

Example 1: As a first example, we consider a fifth-order ($M = N = 6$) elliptic SC filter, having normalized ($\omega/2\pi$) edge frequencies at $\omega_p = 0.2$ and $\omega_s = 0.3$ and ripples $\delta_p = 0.109$ and $\delta_s = 4.68 \times 10^{-4}$ [18]. In this case, $\overline{a} = 0.0506$ and $\overline{b} = 1.80$, giving $\sigma_a = 5.06 \times 10^{-5}$ and $\sigma_b = 1.80 \times 10^{-3}$. The results are displayed in Fig. 3(a) for the mean and in Fig. 3(b) for the standard deviation, respectively, of $|\Delta H(\omega)|$. Notice the

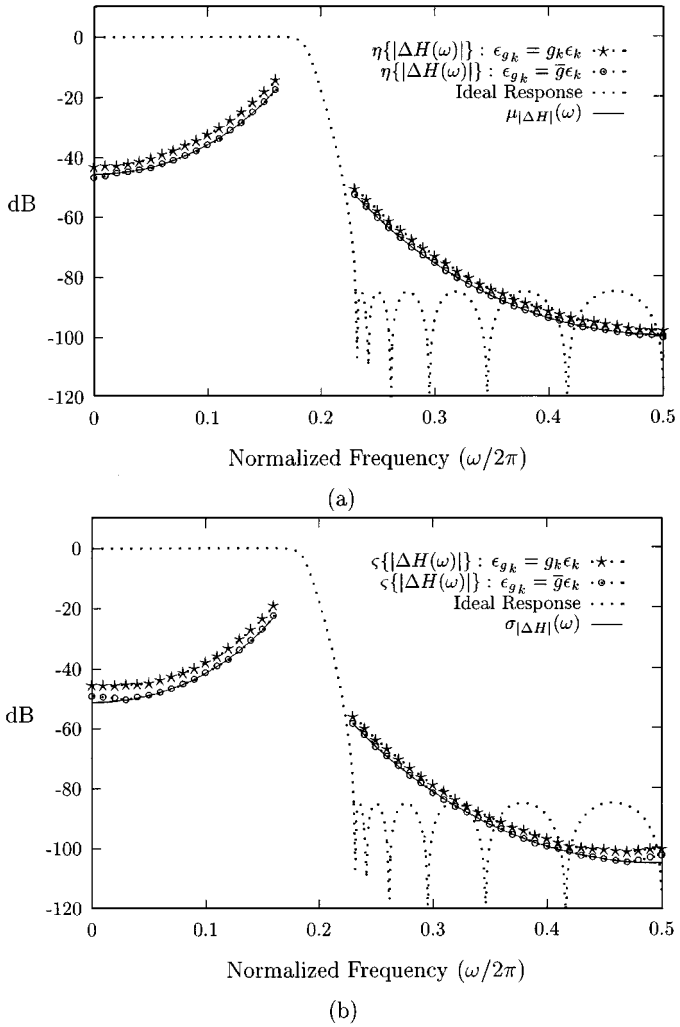

Fig. 4. Theoretical (solid lines) and Monte Carlo ("⋆" and "∘") estimates for (a) the mean and (b) standard deviation of $|\Delta H(\omega)|$ for the thirteenth-order Chebyshev filter of Example 2. Ideal frequency response shows passband and stopband.

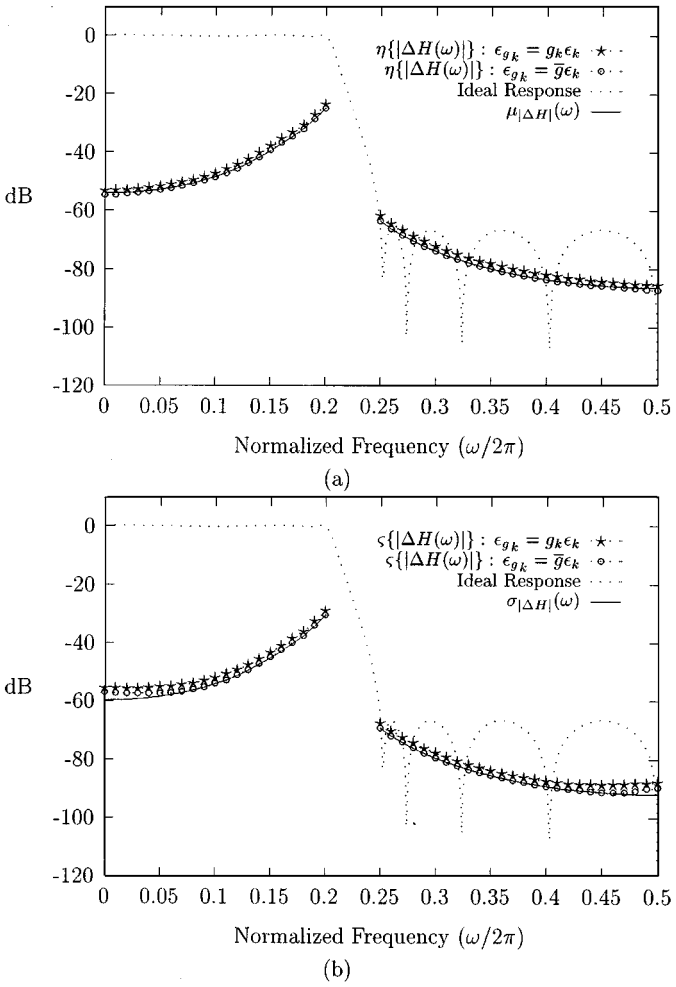

Fig. 5. Theoretical (solid lines) and Monte Carlo ("⋆" and "∘") estimates for (a) the mean and (b) standard deviation of $|\Delta H(\omega)|$ for the filter of Example 3, which considers a transfer function with unequal numerator and denominator orders. Ideal frequency response shows passband and stopband.

perfect agreement between both models ("∘" and "⋆") and between the theory and the Monte Carlo simulations.

Example 2: A thirteenth-order ($M = N = 14$) type II Chebyshev low-pass transfer function is considered next. The main objective of this example is to show the very good accuracy of the proposed theoretical analysis, even when applied to filters with high-order transfer functions and large capacitance spread. The magnitude of the ideal frequency response satisfies the following parameters: $\omega_p = 0.160$, $\omega_s = 0.230$, $\delta_p = 1.15\times10^{-3}$, and $\delta_s = 5.62\times10^{-5}$. Here we have $\overline{a} = 0.0751$ and $\overline{b} = 1.73$, thus $\sigma_a = 7.51\times10^{-5}$ and $\sigma_b = 1.73\times10^{-3}$. The results are shown in Fig. 4(a) and (b). Observe that the theoretical estimates agree perfectly with those obtained by Monte Carlo simulations for the model $\epsilon_{g_k} = \overline{g}\epsilon_k$, verifying the proposed statistical analysis. The small difference between the curves "∘" and "⋆" is due to the large capacitance spread in this case.

Example 3: As a final illustrative example, a transfer function having numerator and denominator polynomials with different orders ($M = 10$ and $N = 6$) is considered. The nominal values of the filter coefficients have been obtained by using the algorithm described in [18], satisfying the specifications $\omega_p = 0.200$, $\omega_s = 0.250$, $\delta_p = 0.0488$, and $\delta_s = 4.47\times10^{-4}$. For this case, $\overline{a} = 0.111$ and $\overline{b} = 1.08$, yielding $\sigma_a = 1.11\times10^{-4}$ and $\sigma_b = 1.08\times10^{-3}$. Again, as shown in Fig. 5(a) and (b), theoretical results are in excellent agreement with Monte Carlo simulations. Notice that in this example, $\overline{b} = 9.73\overline{a}$, indicating that the assumption $\overline{b} \gg \overline{a}$, used in the derivation of (12), is a sufficient but not necessary condition.

B. Probability Distribution Function of $|\Delta H(\omega)|$

Equations (12)–(15), the above examples, and more extensive simulations have indicated that $|\Delta H(\omega)|$ is, at each frequency ω, a Rayleigh random variable that has a probability density function given by

$$f_{|\Delta H(\omega)|}(x) = \begin{cases} (2x/\lambda(\omega))\exp\{-x^2/\lambda(\omega)\}, & x \geq 0 \\ 0, & x < 0 \end{cases} \tag{18}$$

where

$$\lambda(\omega) = \begin{cases} \sigma_b^2(N-1)/|B(\omega)|^2, & \omega \in \Omega_p \\ \sigma_a^2 M/|B(\omega)|^2, & \omega \in \Omega_s. \end{cases} \tag{19}$$

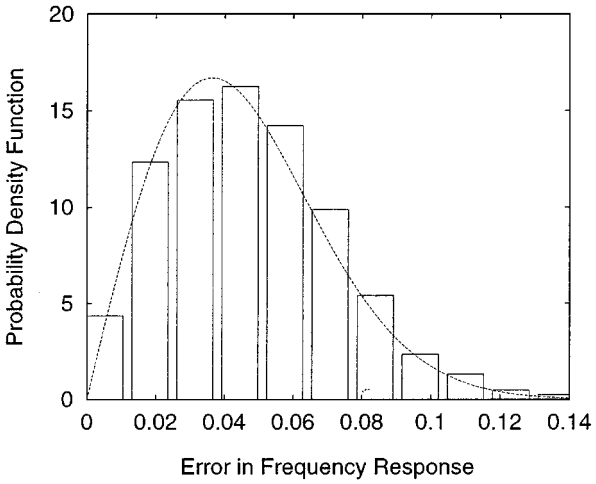

Fig. 6. Histogram of $|\Delta H(\omega)|$ evaluated at $\omega = \omega_p = 0.2$ for 1000 filter samples of Example 1. Broken line indicates the Rayleigh probability density function given by (18).

Fig. 6 displays a histogram for $|\Delta H(\omega)|$ at $\omega = \omega_p = 0.2$ obtained with 1000 Monte Carlo analyses of the fifth-order elliptic filter considered in Example 1. Also shown, in broken lines, is the probability density function in (18), with $\lambda(0.2) = (1.80 \times 10^{-3})^2 \cdot (6-1)/|B(0.2)|^2 = 2.63 \times 10^{-3}$. Fig. 6 shows that the theoretical density function (18) provides a good fit of the one estimated by the Monte Carlo computations and will be used in Section VI to obtain design yield.

V. Achievable Stopband Attenuation

In the ideal case $|H(\omega_s)| = \delta_s$, but because of the random capacitance ratio errors, the actual magnitude at the stopband edge frequency $|\hat{H}(\omega_s)|$ is expected to increase, that is, $\mu_{|\hat{H}|}(\omega_s) > \delta_s$. In some applications, such as in the design of SC decimation filters [11], [28], this may lead to excessive aliasing distortion. It is, therefore, of interest to evaluate the expected value of $|\hat{H}(\omega_s)|$. An upper bound for $\mu_{|\hat{H}|}(\omega_s)$ can be obtained by writing initially, from the first equality in (8)

$$\mu_{|\hat{H}|}(\omega) \le |H(\omega)| + \mu_{|\Delta H|}(\omega). \tag{20}$$

Now substituting (13) into (20), and using the identity $|H(\omega_s)| = \delta_s$, yields

$$\mu_{|\hat{H}|}(\omega_s) \le \delta_s + \frac{\sigma_a \sqrt{\pi M}}{2|B(\omega_s)|} \doteq \delta_{s,\max}. \tag{21}$$

Expressing δ_s in terms of the other filter parameters (M, δ_p, ω_s, and ω_p), the upper bound $\delta_{s,\max}$ can be plotted as a function of any of these parameters. Approximate expressions exist for Butterworth, Chebyshev, and elliptic transfer functions [29], [30], allowing closed analytical formulas for $\delta_{s,\max}$. The procedure is next illustrated for elliptic and Chebyshev filters.

Fig. 7 shows, in solid lines, upper bounds for the stopband attenuation that would be obtained by direct-form SC elliptic filters having $\sigma_\epsilon = 0.001$, $\delta_p = 0.0559$, $\omega_p = 0.227$, and two different values of transition ratio $k = \omega_p/\omega_s$: $k = 0.80$ and $k = 0.85$. These curves indicate that an increase in the filter order ($M-1$) may provide some compensation for the capacitance ratio error effects, although the price to be paid could be quite high for the resulting benefits. For $k = 0.85$, for instance, augmenting the filter order from 8 to 12 leads to an increase of approximately 10 dB in the stopband attenuation, while in the ideal case, shown with a dotted line, this improvement is obtained by increasing the filter order by 1. In some cases, increasing the filter order as an attempt to compensate for the influence of the capacitance ratio errors may even decrease the stopband attenuation, since $\delta_{s,\max}$ is directly proportional to M. This is illustrated in Fig. 8 for Chebyshev filters with $\delta_p = 0.0559$, $\omega_p = 0.17$, and transition ratios $k = 0.70$ and $k = 0.80$. Observe that in the presence of capacitance ratio errors, direct-form SC Chebyshev filters with $k = 0.80$ and order greater than 10 should be avoided, since another Chebyshev filter can be found with smaller order that provides approximately the same stopband attenuation. The attenuation of 40 dB, for instance, can be achieved with orders 9 and 14.

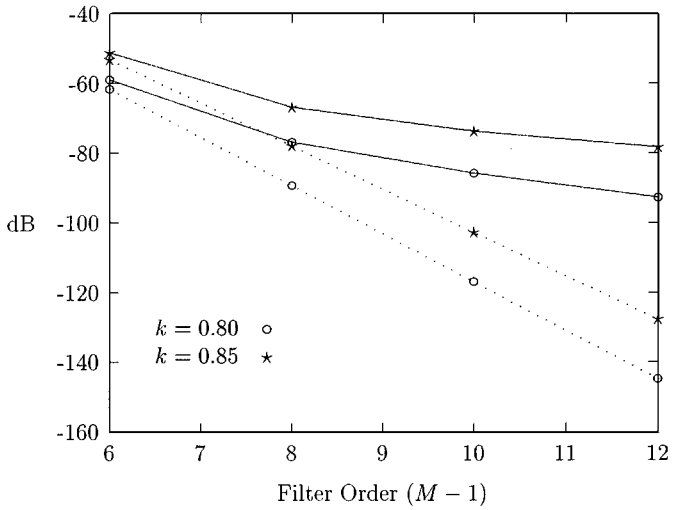

Fig. 7. Dotted lines: stopband amplitudes of ideal elliptic filters; solid lines: upper bounds for stopband amplitudes of direct-form SC elliptic filters having random capacitance ratio errors.

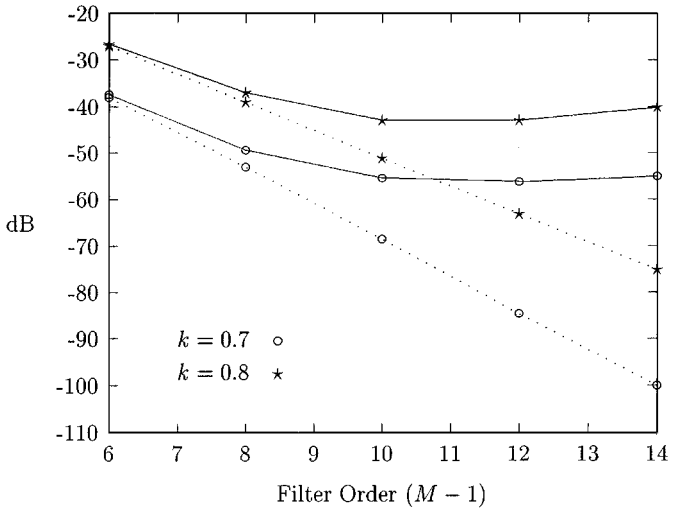

Fig. 8. Dotted lines: stopband amplitudes of ideal Chebyshev filters; solid lines: upper bounds for stopband amplitudes of direct-form SC Chebyshev filters having random capacitance ratio errors.

TABLE I
THEORETICAL AND EXPERIMENTAL RESULTS FOR THE ELLIPTIC FILTERS OF FIG. 4

k	$M-1$	$\overline{a}$	$\overline{b}$	$\lvert B(\omega_s)\rvert$	δ_s $\times 10^{-6}$	$\mu_{\lvert\Delta H\rvert}(\omega_s)$ $\times 10^{-4}$	$\eta\{\Delta H(\omega_s)\}$ $\times 10^{-4}$	$\eta\{\lvert\hat{H}(\omega_s)\rvert\}$ $\times 10^{-4}$
0.80	6	0.4980	8.992	4.472	822.2	2.611	2.608	9.490
	8	0.2316	19.77	5.613	34.28	1.097	1.095	1.150
	10	0.1200	45.98	7.041	1.413	0.5008	0.4954	0.4955
	12	0.06431	111.2	8.839	0.05821	0.2325	0.2320	0.2320
0.85	6	0.5383	8.721	2.257	2188	5.593	5.601	22.30
	8	0.2788	19.08	2.266	125.9	3.271	3.274	3.462
	10	0.1514	44.02	2.267	7.244	1.962	1.948	1.949
	12	0.08502	105.5	2.270	0.4170	1.198	1.202	1.202

TABLE II
THEORETICAL AND EXPERIMENTAL RESULTS FOR THE CHEBYSHEV FILTERS OF FIG. 5

k	$M-1$	$\overline{a}$	$\overline{b}$	$\lvert B(\omega_s)\rvert$	δ_s $\times 10^{-4}$	$\mu_{\lvert\Delta H\rvert}(\omega_s)$ $\times 10^{-4}$	$\eta\{\Delta H(\omega_s)\}$ $\times 10^{-4}$	$\eta\{\lvert\hat{H}(\omega_s)\rvert\}$ $\times 10^{-4}$
0.70	6	0.1667	0.4616	4.118	125.9	9.488	9.527	126.0
	8	0.1344	0.6250	3.133	22.39	11.40	11.42	24.23
	10	0.1099	0.8751	2.434	3.758	13.27	13.23	13.64
	12	0.08959	1.265	1.931	0.5957	14.82	14.79	14.80
	14	0.07750	1.805	1.498	0.1000	17.75	17.78	17.78
0.80	6	0.1887	0.4750	2.168	446.7	20.41	20.67	446.9
	8	0.1507	0.6665	1.366	112.2	29.33	29.37	114.7
	10	0.1255	0.9442	0.8636	27.86	42.72	42.71	49.69
	12	0.1089	1.345	0.5434	6.998	64.03	63.88	64.16
	14	0.09670	1.938	0.3418	1.758	97.11	97.83	97.83

All results presented in Figs. 7 and 8 have been experimentally verified by Monte Carlo simulations, which are summarized in Tables I and II, where $\eta\{|\Delta H(\omega_s)|\}$ is as defined in (16), and $\eta\{|\hat{H}(\omega_s)|\} = \sum_{k=1}^{K} |\hat{H}_k(\omega_s)|/K$. Notice the very close agreement between the theoretical estimate $\mu_{|\Delta H|}(\omega_s)$ and the corresponding Monte Carlo estimate $\eta\{|\Delta H(\omega_s)|\}$. Equally good results, not included in Tables I and II, have been obtained for the standard deviation estimates $\sigma_{|\Delta H|}(\omega_s)$ and $\varsigma\{|\Delta H(\omega_s)|\}$.

A. An Estimate for the Stopband Attenuation

Tables I and II also show that (21) gives a tight upper bound for the actual stopband attenuation, since $\delta_{s,\max} = \delta_s + \mu_{|\Delta H|}(\omega_s)$ is very close to the Monte Carlo estimate $\eta\{|\hat{H}(\omega_s)|\}$. Observe that as the filter order increases, for a fixed transition ratio k, the value of δ_s decreases to a point where $\delta_{s,\max} \approx \mu_{|\Delta H|}(\omega_s)|$, which can then be used as an estimate for the expected stopband attenuation, i.e.,

$$\mu_{|\hat{H}|}(\omega_s) \approx \mu_{|\Delta H|}(\omega_s) = \frac{\sigma_a \sqrt{\pi M}}{2|B(\omega_s)|}. \tag{22}$$

In such case, the stopband attenuation decreases 6 dB as σ_ϵ ($= \sigma_a/\overline{a}$) doubles. Returning to the Chebyshev filter of Example 2, with $M = 14$, $\sigma_\epsilon = 0.001$, $\overline{a} = 0.0751$, $\delta_s = 5.62 \times 10^{-5}$, and $\omega_s = 0.23$, we have $\mu_{|\Delta H|}(0.23) = 2.29 \times 10^{-3} \gg \delta_s$. Thus, according to (22), $\mu_{|\hat{H}|}(0.23) \approx 2.29 \times 10^{-3}$, showing that instead of the desired stopband attenuation of 85 dB one would obtain approximately 52.8 dB in an actual SC implementation. This is a reduction of 32.2 dB due to capacitance mismatch alone. Therefore, using (22), we conclude that the stopband attenuation could be corrected to the desired value by reducing the standard deviation of the capacitance ratio errors by a factor of approximately 64, that is, $\sigma_\epsilon = 0.001/64 = 1.56 \times 10^{-5}$. In fact, the Monte Carlo estimate in this case gives $\log_{10}(\eta\{|\hat{H}(0.23)|\}) = -84.0$ dB. However, the required σ_ϵ is not realizable for SC filters in today's integrated circuit technology, whereas in digital filters this figure could be easily achieved by implementing each filter coefficient with approximately 16 bits. Alternatively, the performance of direct-form SC filters can be improved in the stopband, as well as in the passband, if one considers transfer functions with $M \neq N$, as shown next.

VI. OPTIMUM DESIGN AND YIELD CONSIDERATIONS

For a large class of sampled-data filters, such as the classical Butterworth, Chebyshev, and elliptic filters, considered in the previous section, the numerator and denominator polynomials have the same order, that is, $M = N$. There are some design procedures, however, based on optimized positioning of poles and zeros, that lead to polynomials with unequal orders [18]. As shown next, they also offer the possibility of choosing numerator and denominator orders in such a way that a small deviation is obtained in the frequency response.

Usually, the frequency response deviation in the passband increases as the denominator order increases, as indicated by (12) and (14), since N increases and $|B(\omega)|$ decreases for $\omega \in \Omega_p$, because the distance from the poles to the unit circle in the passband is less than *one*. Exceptions may occur for wide-band fil-

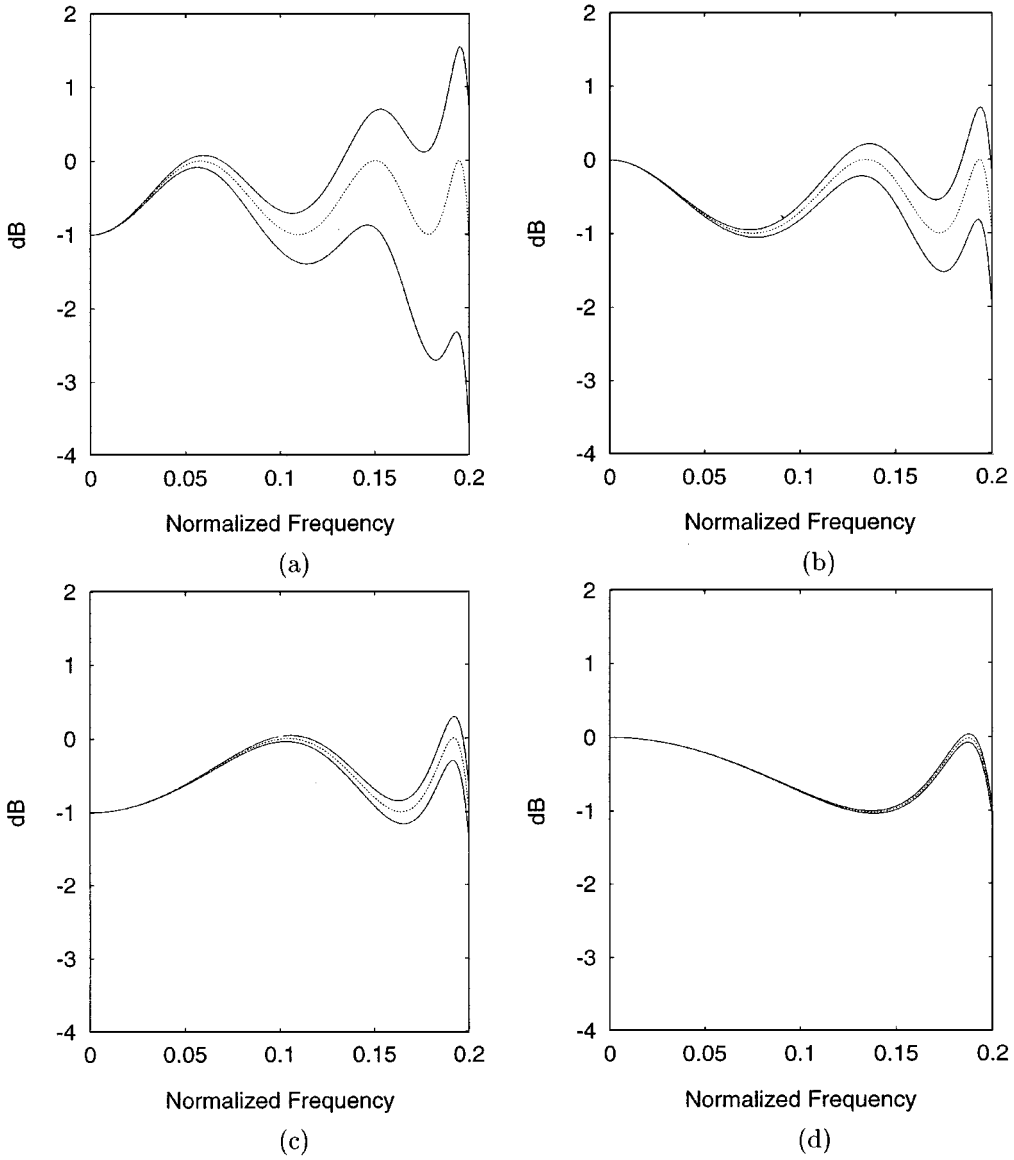

Fig. 9. Passband sensitivity characteristics of direct-form recursive SC filters with $\omega_p = 0.2, \omega_s = 0.3, \delta_p = 0.1087$, and $\delta_s < 0.001$. (a) $M = 5, N = 7$; (b) $M = 6, N = 6$; (c) $M = 7, N = 5$; (d) $M = 9, N = 3$. Dotted lines: ideal frequency response; solid lines: boundary curves $\beta_\ell(\cdot)$ and $\beta_u(\cdot)$.

ters. In this case, some inner poles of the classical elliptic approximation are so far from the unit circle that they can be moved to the origin, almost without modifying the filter frequency response, resulting in transfer functions with $N < M$. In [18], the transfer function sensitivities of digital filters have been computed and compared for several values of N and M for a given specification. However, only the peak of the worst case sensitivities for the poles closest to the unit circle have been computed. A more comprehensive comparison is provided below for SC filters.

A. Boundary Curves for the Feasible Frequency Responses

From (8), the following bounds can be written for the actual transfer function

$$|H(\omega)| - |\Delta H(\omega)| \le |\hat{H}(\omega)| \le |H(\omega)| + |\Delta H(\omega)| \quad (23)$$

for all ω. On the other hand, using the probability density function given by (18), the probability that $|\Delta H(\omega)|$ attains values within a certain interval can be readily computed. In particular

$$P\{|\Delta H(\omega)| \le r\sigma_{|\Delta H|}(\omega)\} = \int_0^{r\sigma_{|\Delta H|}(\omega)} f_{|\Delta H(\omega)|}(x)\,dx = 1 - \exp\{(\pi/4 - 1)r^2\} \quad (24)$$

where r is a real positive number. Since for $r = 5$, the above probability is equal to 0.995, it follows that with high probability

$$\beta_\ell(\omega) \le |\hat{H}(\omega)| \le \beta_u(\omega) \quad (25)$$

where

$$\beta_\ell(\omega) = |H(\omega)| - 5\sigma_{|\Delta H|}(\omega) \quad (26)$$

TABLE III
FREQUENCY RESPONSE DEVIATION IN THE STOPBAND OF FILTERS WITH $\omega_p = 0.2$, $\omega_s = 0.3$, $\delta_p = 0.1087$, AND $\delta_s < 0.001$

$M-1$	$N-1$	$\bar{a}$	$\bar{b}$	$\lvert B(\omega_s)\rvert$	δ_s $\times 10^{-4}$	$\mu_{\lvert\Delta H\rvert}(\omega_s)$ $\times 10^{-5}$	$\eta\{\Delta H(\omega_s)\}$ $\times 10^{-5}$	$\eta\{\lvert\hat{H}(\omega_s)\rvert\}$ $\times 10^{-4}$
4	6	0.03152	2.904	3.239	4.677	1.929	1.957	4.898
5	5	0.05060	1.804	2.309	4.677	4.757	4.628	4.732
6	4	0.08275	1.128	1.652	4.571	11.74	11.35	5.754
8	2	0.13790	0.6508	1.103	8.222	33.24	32.10	11.48

and

$$\beta_u(\omega) = |H(\omega)| + 5\sigma_{|\Delta H|}(\omega). \tag{27}$$

Equations (26) and (27) determine, respectively, the lower and upper boundary curves that enclose the feasible frequency responses. For ω in Ω_p, for instance, (14) can be combined with (26) and (27) to define the boundary responses in the passband. In view of the accuracy of the theoretical analysis verified in the previous sections, these boundaries provide quick and reliable yield evaluation at any particular frequency of interest, for a specification window of acceptance defined in the frequency response. The proportion of the feasible frequency responses that pass this specification window test is the most commonly understood meaning of design (or parametric) yield [31]. For detailed treatment and formal definition of yield evaluation and estimation, from the design stage to the integrated circuit production cycle through final test, see, e.g., [17] and [32]. The following example illustrates the procedure of finding an optimum design, so that yield is maximized by comparing the boundary curves obtained for each filter.

B. Illustrative Example and Discussion

Fig. 9 shows the boundary curves $\beta_\ell(\cdot)$ and $\beta_u(\cdot)$ in the passband of four different designs: (a) $M = 5$, $N = 7$; (b) $M = 6$, $N = 6$; (c) $M = 7$, $N = 5$; and (d) $M = 9$, $N = 3$. In all cases, $\sigma_\epsilon = 0.001$, $\omega_p = 0.2$, $\omega_s = 0.3$, $\delta_p = 0.1087$ (passband ripple of 1 dB), and $\delta_s = 0.001$ (stopband attenuation of 60 dB) [18]. Each plot displays three curves: the ideal frequency response in dotted lines and the boundary curves in solid lines. Note that the decrease of N reduces the sensitivity in the passband, as expected. At the passband edge frequency, for example, $\mu_{|\Delta H|}(0.2) = 0.04554$ and $\sigma_{|\Delta H|}(0.2) = 0.02381$, for the fifth-order elliptic filter [$M = N = 6$; Fig. 9(b)], and $\mu_{|\Delta H|}(0.2) = 3.674 \times 10^{-3}$ and $\sigma_{|\Delta H|}(0.2) = 1.921 \times 10^{-3}$, for the least sensitive filter [$M = 9$, $N = 3$; Fig. 9(d)]. However, the necessary increase of M to maintain high stopband attenuation tends to increase the frequency response deviation in the stopband, as indicated in (13) and (15). Moreover, $|B(\omega)|$ decreases in the stopband as the number of poles decreases, since in this example the distance from most poles to the unit circle region corresponding to stopband frequencies is greater than *one*. This is indicated by $|B(\omega_s)|$ in Table III, as N decreases from 7 to 3. Nevertheless, high stopband attenuation can be achieved in all cases of the example. For the case $M = 9$, $N = 3$, the achievable stopband attenuation is expected to be, from (21), about 59 dB.

The price for achieving the lowest passband sensitivity is a longer delay line, since the fifth-order elliptic filter would require five unit delays, while the least sensitive one would require eight unit delays to implement the forward path coefficients, as indicated in Fig. 10(a). Alternatively, since in the latter case the order of the numerator is four times the order of the denominator, five second-order FIR SC cells with almost identical direct-form topologies can be used: four cascaded cells in the forward path and one cell in the feedback path, as illustrated in Fig. 10(b). The resulting structure shows a high degree of modularity and, hence, is attractive for VLSI implementation. Moreover, each FIR cell can be implemented by a single multiplexed op-amp [3], [12]. It should also be observed that this structure has the passband sensitivity of Fig. 9(d), since its poles are still implemented in direct form, as shown in Fig. 10(b). Particular circuit diagrams and specific practical design considerations are beyond the scope of this paper and can be found elsewhere [12].

A linear phase FIR filter satisfying the above specifications would require a delay line at least 21 units long. In some applications, where it is sufficient to approximate linear phase over a fraction of the passband only [33], properly designed recursive SC filters may replace with advantages a linear phase FIR SC filter. Fig. 11 shows the group delays obtained for the filters considered in the above example. It can be observed that the filter having $M = 9$, $N = 3$ (in solid line) has an approximately constant group delay in most of the passband, due to the fact that it has only two poles, which are not as close to the unit circle as the ones of the other filters. This comparative study suggests that when exactly linear phase is not necessary, it may be more efficient to implement a direct-form recursive SC filter with a reduced number of poles than a linear phase FIR SC filter.

A link can also be established between the analysis proposed in this paper and capacitance sizing so that capacitance matching and noise can be optimized. Once the unit capacitance ratio tolerance σ_ϵ is obtained for a certain performance in the passband, through (26) and (27), and in the stopband, through (22), then the unit capacitor size can be defined according to the uncertainty parameters specified by the process of fabrication. Consequently, all other capacitor sizes, and noise generated by them, can be determined by applying the corresponding scaling factor. There exists a tradeoff, therefore, that determines an upper bound for numerator and denominator orders, and a lower bound for capacitor sizes, in the benefit of low sensitivity and noise. Increasing capacitor dimensions, on the other hand, also leads to higher power consumption, since the operational amplifiers will have to drive larger capacitive loads.

VII. CONCLUDING REMARKS

This paper considered the effects of random capacitance ratio errors in the frequency response of direct-form recursive SC

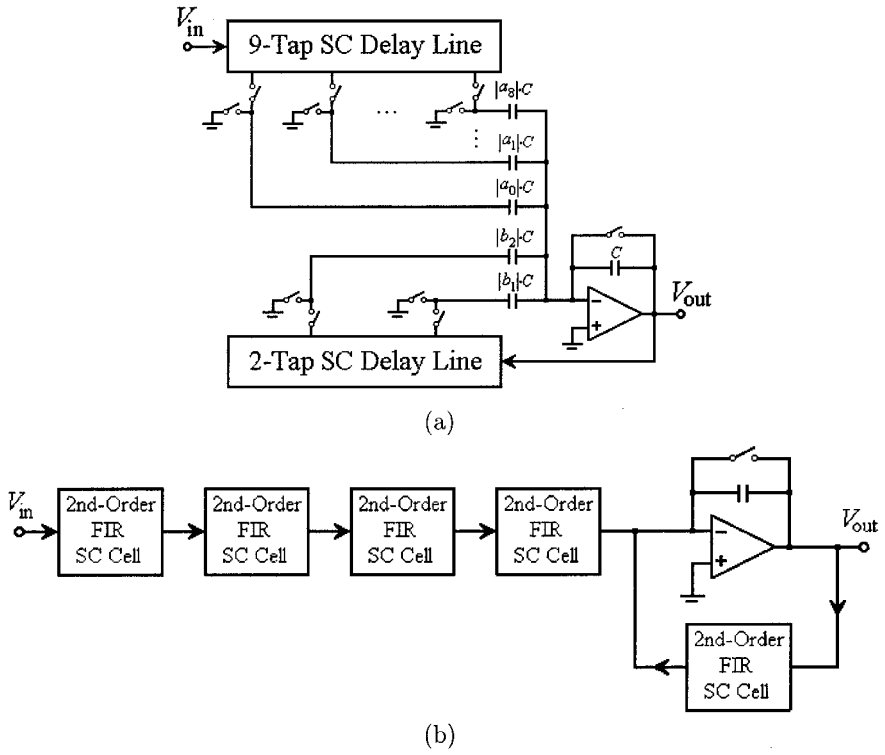

Fig. 10. Two realizations of the least sensitive filter in Fig. 9(d). (a) Using two delay lines, as in Fig. 1(b). (b) Using second-order SC FIR cells as basic building blocks.

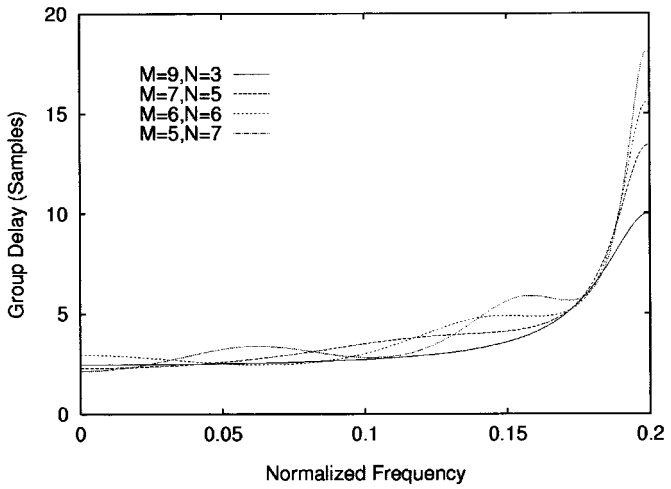

Fig. 11. Group delay responses of the filters in Fig. 9.

filters, an issue of increasing importance in view of the trends toward equipment miniaturization and consequent reduction in process dimensions into the deep submicrometer range. As a result of the statistical analysis, closed-form expressions for the mean and the standard deviation of the error in the frequency response were obtained. Extensive Monte Carlo simulations were carried out to verify the main theoretical results and the model used for random capacitance ratio errors.

An estimate for the stopband attenuation was derived, allowing the designer to predict, for instance, the necessary capacitance ratio tolerance for a given filter to attain a specified stopband attenuation. Several such estimates were presented for elliptic and Chebyshev filters, showing, in particular, that while in the ideal case an arbitrarily large stopband attenuation can be achieved by simply augmenting the filter order, in a more realistic situation, due to random capacitance ratio errors, an increase in the filter order may even lead to a decrease in the stopband attenuation.

The obtained probability density function of the error in the frequency response was used to evaluate the design yield. Through an illustrative example, it was shown how this can be incorporated into an efficient algorithm that considers transfer functions with equal or unequal numerator and denominator orders to design direct form recursive SC filters that simultaneously achieve low passband sensitivity and large stopband attenuation.

This paper does not intend to suggest the recursive direct-form structure as a solution for the general SC filter design problem. However, by a judicious evaluation of the revealed quantitative tradeoffs, allied to a simplicity of design and layout implementation, this fundamental class of filters can be considered as an alternative viable solution, and its effectiveness can be maintained relative to more complex filter structures in some interesting applications. Such is the essential aim of this paper.

Although the main concern was with respect to SC filters, the approach advanced here can be applied to any filter technique in which coefficient errors have a Gaussian distribution, such as those considered in Section II.

REFERENCES

[1] T. Enomoto, T. Ishihara, and M. Yasumoto, "Integrated tapped MOS analogue delay line using switched-capacitor technique," *Electron. Lett.*, vol. 18, pp. 193–194, Mar. 1982.

[2] Y. S. Lee and K. W. Martin, "A switched-capacitor realization of multiple FIR filters on a single chip," *IEEE J. Solid-State Circuits*, vol. 23, pp. 536–542, Apr. 1988.
[3] G. Fischer, "Switched-capacitor FIR filters—A feasibility study," *IEEE Trans. Circuits Syst. II*, vol. 41, pp. 823–827, Dec. 1994.
[4] B. C. Rothemberg, S. H. Lewis, and P. J. Hurst, "A 20-Msample/s switched-capacitor finite-impulse-response filter using a transposed structure," *IEEE J. Solid-State Circuits*, vol. 30, pp. 1350–1356, Dec. 1995.
[5] A. Fettweis and H. Wupper, "A solution to the balancing problem in N-path filters," *IEEE Trans. Circuit Theory*, pp. 403–405, May 1971.
[6] I. A. Young, D. A. Hodges, and P. R. Gray, "MOS switched-capacitor analog sampled-data direct-form recursive filters," *IEEE J. Solid-State Circuits*, vol. SC-14, pp. 1020–1033, Dec. 1979.
[7] P. V. A. Mohan, V. Ramachandran, and M. N. S. Swamy, *Switched-Capacitor Filters—Theory, Analysis and Design*. Englewood Cliffs, NJ: Prentice-Hall, 1995, pp. 189–193.
[8] Y. Hirata, K. Kato, N. Takahashi, and T. Takebe, "High frequency switched capacitor IIR filters using parallel cyclic circuits," in *Proc. IEEE Int. Symp. Circuits Syst.*, San Diego, CA, May 1992, pp. 1199–1202.
[9] C.-A. Gobet, S. K. Mitra, and A. Petraglia, "Low-passband sensitivity switched capacitor filters using a parallel connection of two structurally lossless networks," *Int. J. Circuit Theory Applicat.*, vol. 20, pp. 47–62, Jan./Feb. 1992.
[10] F. A. P. Barúqui, A. Petraglia, S. K. Mitra, and J. E. Franca, "Switched-capacitor decimation filter for 0.8 μm CMOS," in *Proc. IEEE Int. Symp. Circuits and Systems*, Monterey, CA, May/June 1998, pp. I.496–I.499.
[11] A. Petraglia and J. S. Pereira, "Switched-capacitor decimation filters with direct-form polyphase structure having very small sensitivity characteristics," in *Proc. IEEE Int. Symp. Circuits and Systems*, Orlando, FL, May 1999, pp. II.73–II.76.
[12] J. S. Pereira and A. Petraglia, "Low sensitivity direct-form IIR SC filters with improved phase linearity," in *Proc. IEEE Int. Symp. Circuits Syst.*, Geneva, Switzerland, May 2000, pp. III.169–III.172.
[13] A. Gersho, "Charge-transfer filtering," *Proc. IEEE*, vol. 67, pp. 196–218, Feb. 1979.
[14] J. H. Fischer, "Noise sources and calculation techniques for switched-capacitor filters," *IEEE J. Solid-State Circuits*, vol. SC-17, pp. 742–752, Aug. 1982.
[15] J.-B. Shyu, G. C. Temes, and K. Yao, "Random errors in MOS capacitors," *IEEE J. Solid-State Circuits*, vol. SC-17, pp. 1070–1075, Dec. 1982.
[16] W. W. Poliscuk and B. L. Rojo, "A note on statistical sensitivity computation in switched-capacitor networks," *IEEE Trans. Circuits Syst.*, vol. 35, pp. 423–425, Apr. 1988.
[17] K. R. Laker and W. M. C. Sansen, *Design of Analog Integrated Circuits and Systems*. New York: McGraw-Hill, 1994, pp. 226–231, 696–703.
[18] L. B. Jackson, "An improved Martinez/Parks algorithm for IIR design with unequal number of poles and zeros," *IEEE Trans. Signal Processing*, vol. 29, pp. 1234–1238, May 1994.
[19] M. J. McNutt, S. LeMarquis, and J. L. Dunkley, "Systematic capacitance matching errors and corrective layout procedures," *IEEE J. Solid-State Circuits*, vol. 29, pp. 611–616, May 1994.
[20] J.-B. Shyu, G. C. Temes, and F. Krummenacher, "Random error effects in matched MOS capacitors and current sources," *IEEE J. Solid-State Circuits*, vol. SC-19, pp. 948–955, Dec. 1984.
[21] J. L. McCreary, "A precision measurement technique for capacitor array ratio errors," in *Proc. Eur. Conf. Circuit Theory and Design*: Univ. of Stuttgart, Germany, Sept. 1983, pp. 230–232.
[22] O. A. Palusinski, D. M. Gettman, D. Anderson, H. Anderson, and C. Marcjan, "Filtering applications of filed programmable analog arrays," *J. Circuits, Syst. Comput.*, vol. 8, pp. 337–353, 1998.
[23] C. M. Puckette, W. J. Butler, and D. A. Smith, "Bucket brigade transversal filters," *IEEE Trans. Commun.*, vol. COM-22, pp. 926–934, July 1974.
[24] A. Petraglia and S. K. Mitra, "Effects of coefficient inaccuracy in switched-capacitor transversal filters," *IEEE Trans. Circuits Syst.*, vol. 38, pp. 977–983, Sept. 1991.
[25] A. Petraglia, "Coefficient inaccuracy effects in recursive analog sampled-data filters," in *Proc. IEEE Int. Symp. Circuits and Systems*, Chicago, IL, May 1993, pp. 1030–1033.
[26] Y. Tsividis, "Signal processors with transfer function coefficients determined by timing," *IEEE Trans. Circuits Syst.*, vol. CAS-29, pp. 807–816, Dec. 1982.
[27] A. Petraglia, "Frequency response deviation in switched-capacitor filters caused by random MOS capacitance errors," in *Proc. IEEE Int. Symp. Circuits Syst.*, Hong Kong, June 1997, pp. 125–128.
[28] J. E. Franca, A. Petraglia, and S. K. Mitra, "Multirate analog-digital systems for signal processing and conversion," *Proc. IEEE*, vol. 85, pp. 242–264, Feb. 1997.
[29] J. E. Storer, *Passive Network Synthesis*. New York: McGraw-Hill, 1957, pp. 287–302.
[30] A. H. Gray Jr. and J. D. Markel, "A computer program for designing digital elliptic filters," *IEEE Trans. Acoust., Speech, Signal Processing*, vol. ASSP-24, pp. 529–538, Jun. 1976.
[31] M. A. Styblinsky and L. J. Opalsky, "Algorithms and software tools for IC yield optimization based on fundamental fabrication parameters," *IEEE Trans. Computer-Aided Design*, vol. CAD-5, pp. 79–89, Jan. 1986.
[32] W. Maly, A. J. Strojwas, and S. W. Director, "VLSI yield prediction and estimation: A unified framework," *IEEE Trans. Computer-Aided Design*, vol. CAD-5, pp. 114–130, Jan. 1986.
[33] H. Baher and M. O'Malley, "Design of switched-capacitor and wave digital filters with linear phase and amplitude selectivity," *IEEE Trans. Circuits Syst.*, vol. 37, pp. 614–622, May 1990.

Antonio Petraglia (S'89–M'91–SM'99) received the Engineer and M.S. degrees from the Federal University of Rio de Janeiro (UFRJ), Brazil, in 1977 and 1982, respectively, and the Ph.D. degree from the University of California, Santa Barbara, in 1991, all in electrical engineering.

In 1979, he joined the Faculty of UFRJ as an Associate Professor of electrical engineering, where he served as Co–Chair of the Department of Electronic Engineering from 1982 to 1984. During the second semester of 1991, he was a post-Doctoral researcher with the Department of Electrical and Computer Engineering, University of California, Santa Barbara, working on digital equalizers for professional audio. Since 1992, he has been on the Faculty of the Program for Post-Graduate Engineering at UFRJ, where, in 1997 he established the Laboratory for the Processing of Analog and Digital Signals. He is currently a visiting scholar with the Electrical Engineering Department, University of California, Los Angeles. He has been involved in teaching and research activities in the areas of mixed analog–digital integrated circuit design, including filters and radio-frequency front-end components for communication applications.